

# Development of Artificial Intelligence as a Conversion Tool for Cine Electronic Portal Imaging Device Images to Radiotherapy Dosimetry: Preliminary Study

Muhammad Mahdi Ramadhan<sup>1</sup>, Wahyu Edy Wibowo<sup>2</sup>, Supriyanto Ardjo Pawiro<sup>1\*</sup>

1. Department of Physics, Faculty of Mathematics and Natural Sciences, Universitas Indonesia, Depok, West Java, 16424, Indonesia
2. Department of Radiation Oncology, Cipto Mangunkusumo National General Hospital, Jakarta, 10430, Indonesia

ARTICLE INFO	ABSTRACT
<p><b>Article type:</b> Original Paper</p> <hr/> <p><b>Article history:</b> Received: Oct 11, 2021 Accepted: Feb 18, 2022</p> <hr/> <p><b>Keywords:</b> Radiotherapy In Vivo Dosimetry Artificial Intelligence</p>	<p><b>Introduction:</b> This research is a preliminary study of the development of Artificial Intelligence (AI) as a conversion tool from the pixel value of Cine a-Si 1000 Electronic Portal Imaging Device (EPID) images to dose. It also investigates the relationship between the Monitor Unit (MU), dose rate, number of frames, and beam profile of Electronic Portal Imaging Device (EPID) images to facilitate further mathematical correction that must be added to create accurate dosimetry by Cine EPID images.</p> <p><b>Material and Methods:</b> Homogeneous and inhomogeneous phantom was irradiated in a Linear Accelerator (Linac) 6 MV with different techniques, field size, and phantom thickness. The Cine a-Si 1000 EPID images were taken and compared to dose distribution data derived from the Eclipse treatment planning system (TPS) at Source Axis Distance 100 cm or isocenter field. The AI model training process begins with the augmentation of EPID and TPS images from homogeneous phantom so that 1152 images are obtained. These images are then split randomly into training and testing data 7:3, and validation is done using gamma index 3%/3mm.</p> <p><b>Results:</b> An AI model based on Convolutional Neural Network (CNN) with 6 layers has been successfully created that can convert EPID pixel values into dose distribution without any mathematical correction. The best results from validation with a gamma index of 3%/3mm compared to TPS calculations reached 92.40% <math>\pm</math>28.14%.</p> <p><b>Conclusion:</b> An AI model has been successfully created that can convert EPID pixel values into dose distribution but need improvement by considering the characteristics contained in the EPID image and the number of datasets.</p>

► Please cite this article as:

Ramadhan MM, Wibowo WE, Pawiro SA. Development of Artificial Intelligence as a Conversion Tool for Cine Electronic Portal Imaging Device Images to Radiotherapy Dosimetry: Preliminary Study. Iran J Med Phys 2022; 19: 296-304. 10.22038/IJMP.2022.60896.2024.

## Introduction

Verification of a patient's position using dosimetry film requires periodic calibration and takes a long time. The Electronic Portal Imaging Device (EPID) is a tool designed to resolve these issues. The earliest EPID model was a scanning liquid-filled ionization chamber (SLIC), followed by a charge-coupled camera-based device (CCD), with the most recent and widely used EPID being based on amorphous silicon (a-Si) technology (1).

An EPID detector can be easily set up by attaching it to the linear accelerator. It also has a higher resolution and more accurate readings of dose distribution. In addition, it can capture images continuously through its continuous acquisition (cine) mode (2). Previous studies have shown that this mode can be used to track the movement of tumor organs (3).

Dose information acquired through EPID images can be used to verify dose distribution before treatment. In addition, it can also be used as in-vivo

dosimetry (IVD), that is dose verification during treatment (2). Mans et al. found that 9 out of 17 serious errors missed by pre-treatment verification, such as failed plan transfer and delivery, were detected during treatment verification (4). Consequently, many algorithms have been developed to produce IVD based on EPID images (5-11).

The use of EPID images for dosimetry is not without challenges. McCurdie et al summarized those challenges into nine main categories, namely image ghosting, overresponse to low energy photons, self-scatter signals, optical glare effect, patient scattering, robotic arm backscatter, mechanical flexion, gantry angle uncertainties, and lost image dose. Current research aims to solve these challenges so that it is possible to create an accurate dosimetry based on EPID image (12,13).

The techniques to reconstruct dose distribution from EPID images can be classified into three categories: Monte Carlo (MC)-based model,

\*Corresponding Author: Tel: (+62-21) 787 2610; Fax: (+62-21) 7863441; Email: supriyanto.p@sci.ui.ac.id

convolution-based model, and empirical-based model. Each of the categories have has their own advantages and disadvantages. For example, the MC-based model has the highest accuracy but requires a long computing time, which makes it impractical for routine verifications(1).

Currently, researchers are developing radiotherapy tools using artificial intelligence (AI) (14–20). AI works by combining large amounts of data with fast and iterative intelligent processing algorithms. It allows the system to learn automatically from patterns or features in the data (21,22). For EPID dosimetry, researcher have used AI as a correction tool to increase the similarity of dose distribution acquired through EPID (23,24). However, there are no previous research that use AI to reconstruct dose distribution as of this writing.

This study developed AI as a reconstruct dose technique by the conversion of pixel value of EPID images into dose to build accurate two-dimensional radiotherapy dosimetry. To support the results and further improvement, this study will also investigate the relationship between the monitor unit (MU), dose rate, number of frames, and beam profile of an EPID detector in cine mode.

### Materials and Methods

The experiments were performed at Cipto Mangunkusumo General Hospital using a Varian Unique (Varian Medical Systems, Palo Alto, CA, USA) single energy (6 MV) Linac, equipped with an a-Si 1000 EPID. All the images were extracted in cine mode, with a frame rate of 4.711 frames per seconds (fps) at 400 MU/min. The gantry angle was set at 0 degrees, while the source to detector distance (SDD) was set at 150 cm, and the phantom is took placed between the source and detector with the source axis distance (SAD) set to 100 cm as illustrated in Figure 1. The EPID detector specification is shown in Table 1. The images from the EPID were compared with the Digital Imaging and Communications in Medicine (DICOM), which was generated from the Eclipse treatment planning system (TPS), version 13.6 (Varian Unique Medical Systems, Palo Alto, CA, USA) using the anisotropic analytical algorithm (AAA). This research is divided into two stages, namely the development of the AI model and the investigation of cine EPID images characteristics. The flow of this research is shown in Figure 2 and explained in the next stage.

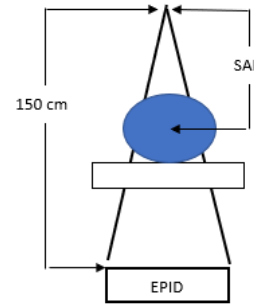


Figure 1. Arrangement between phantom and the EPID in the experiment

Table 1. Specification of the a-Si 1000 EPID

Parameter	Value
Max irradiated area (cm <sup>2</sup> )	30 × 40
Active area (cm <sup>2</sup> )	30 × 40
Total pixel matrix	768 × 1024
Pixel size (mm)	0.390

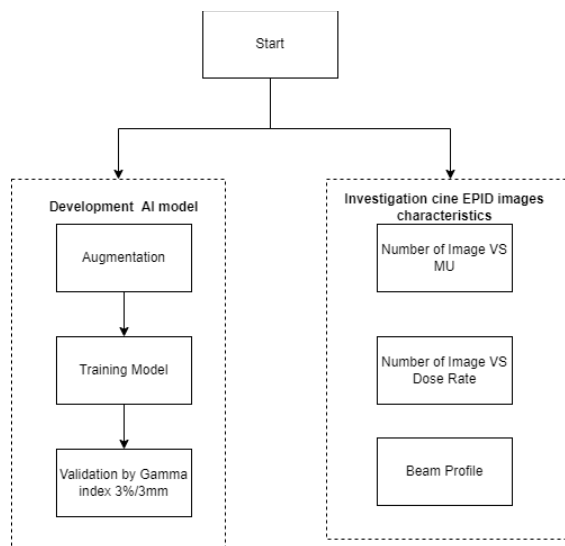


Figure 2. Main workflow of the study

### Development of AI Model Preparation

A homogeneous phantom with RW3 slab phantom from PTW with size 40×40×1 cm<sup>3</sup> was arranged and irradiated with various thicknesses (symbolized by *w*) and field sizes (symbolized by *l*) according to Table 2. Furthermore, the MU and dose rate was set at 100 MU and 400 MU/min, respectively.

Image processing of an EPID image uses a unique calculation technique as shown in Equations (1) and (2).

$$S_{x,y} = 2^n - S_{raw(x,y)} \tag{1}$$

$$S_{\Sigma(x,y)} = \sum_i^m S_i(x,y) \tag{2}$$

where  $S_{raw}$  is the image before processing;  $S$  is the image after processing;  $x$  and  $y$  are index pixel values of an image;  $n$  is the bit value of the image;  $i$  is the index of the number of images;  $m$  is the maximum number of images in one exposure; and  $S_i$  is an image to  $i$ .

Table 2 Variation of thickness ( $w$ ) and field size ( $L$ ) in the homogeneous phantom

L \ W	W			
	5 cm	10 cm	15 cm	20 cm
5×5 cm <sup>2</sup>	✓	✓	✓	✓
10×10 cm <sup>2</sup>	✓	✓	✓	✓
15×15 cm <sup>2</sup>	✓	✓	✓	✓
20×20 cm <sup>2</sup>	✓	✓	✓	✓

Equation 1 is for reversing and offsetting the amount of cine produced by EPID. Each raw pixel value is replaced by  $2^n$  and  $n$  is the bit value. Following research conducted by Peca et al., the bit is 14, it is designed to arrange film with lower pixel values representing a larger dose. Because of that, this equation modifies the increase in intensity linear as increasing the dose (11).

Equation 2 explains about sums up all the cine EPID images in one exposure becoming a single image. It occurs because all images are recorded as a single unit, not individual frames in cine imaging (11). Up to this stage, the image value is still in pixels.

For EPID image validation, calculation simulations were carried out using TPS, and the dose distribution image from TPS calculations was used as ground truth. Because TPS images only can generate on sizes of 384×512. This condition is different from the total pixels in EPID images (see Table 1). In order to facilitate the comparison, the images from TPS and EPID were resized to 384×512, or half the resolution of the EPID images.

### Augmentation

Because the total number of cases is still small, following Table 2 just only 16 cases, then augmentation is needed. The augmentation is done by rotate rotating the image every 5 degrees and flipping it so that 1152 datasets for EPID and TPS images are created. The dataset is divided randomly for training and testing data 7:3.

### Build the AI model

In this study, an Artificial Intelligence (AI) model was created, the model was built using the python programming language, run on Nvidia K80 GPU with 12 GB RAM memory, and the architecture is shown in Table 3 The model used is Convolutional Neural Networks (CNN) with 6 layers. On each layer, there are hidden neurons whose number increases by 2 times on each additional layer, i.e., 16, 32, 64, 128, 256. Then, the last layer (6<sup>th</sup> layer) is the output layer that produces the distribution dose image. We optimize the models by Adam optimizer where the epoch was set to 15 with a learning-rate of 0.000001, and the loss value calculation is represented by mean squared error (MSE).

### Validation

Validation was carried out using the gamma index on the in-house software built by MATLAB R2019b. The gamma index ( $\gamma$ ) is one of the most used metrics for the verification of complex modulated radiotherapy. All dose distributions reconstructed from EPID images are compared with the actual dose distribution from the treatment plan using  $t$ -test. The gamma index criterion used in this study is 3%/3mm.

Table 3. Artificial Intelligence model

Layer	Activity	Dimension	Number of parameter
1	convolution 2D	1,384,512,16	416
	batch normalization	1,384,512,16	64
	activation	1,384,512,16	0
2	convolution 2D	1,384,512,32	12,832
	batch normalization	1,384,512,32	128
	activation	1,384,512,32	0
3	convolution 2D	1,384,512,64	51,264
	batch normalization	1,384,512,64	256
	activation	1,384,512,64	0
4	convolution 2D	1,384,512,128	204,928
	batch normalization	1,384,512,128	512
	activation	1,384,512,128	0
5	convolution 2D	1,384,512,256	819,456
	batch normalization	1,384,512,256	1,024
	activation	1,384,512,256	0
6	convolution 2D	1,384,512,1	6,401
	batch normalization	1,384,512,1	4
	activation	1,384,512,1	0
Total parameters			1,097,285
Trainable parameters			1,096,291
Non-trainable parameters			994

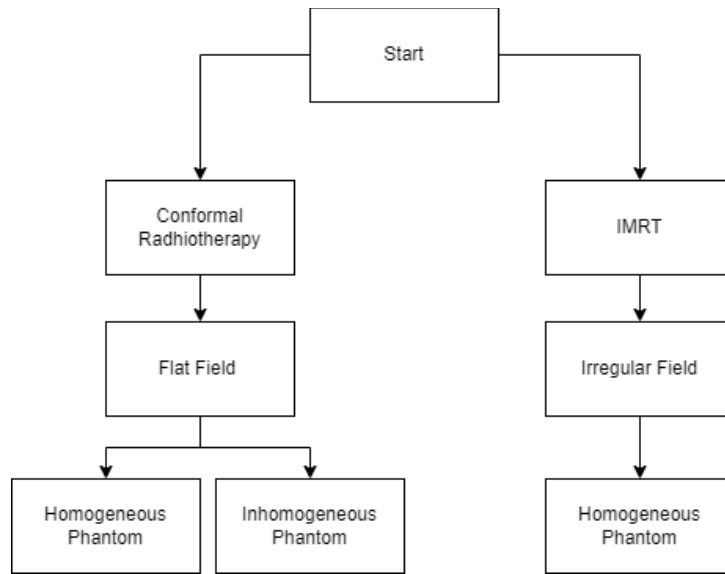


Figure 3. Workflow investigation beam profile



Figure 4. Example of (a) planning on TPS in inhomogeneous phantom; (b) set up Rando phantom and EPID

**Investigation of characteristics of Cine EPID Images**  
**Investigate the number of cine EPID images versus MU**

The settings follow Figure 1, using a homogeneous phantom made from RW3 with a thickness of 10 cm. The presence of the phantom is necessary to reduce the risk of damaging the detector due to high radiation exposure. In this step, a number of EPID images was generated in cine mode with variations of MU between 5 and 300, at a fixed dose rate of 400 MU/minute. This step is needed in order to determine the relationship between the number of cine EPID images and the MU. when the number of EPID images is inconsistent with the increase in the MU value, then the sum of the pixel values of each cine image carried out by equation 2 will also be inconsistent. This can cause the AI model to fail to convert the pixel value into the correct dose.

**Investigate the number of cine EPID images versus dose rate**

The settings are the same as above mentioned. In this step, the phantom was irradiated with a fixed MU of 100 and the dose rate is varied from 100 to 400 MU/min. This investigation checks the consistency of increasing the number of cine EPID images with the dose rate to anticipate errors that will occur in equation 2.

**Investigate beam profile**

The focus of this stage is to investigate the physical process leading to the creation of pixel values in the EPID images. The workflow is shown in Figure 3, divide based on the irradiation technique, namely: conformal radiotherapy and intensity-modulated radiation therapy (IMRT) techniques.

For conformal radiation therapy, two variations of phantom were used. First, a homogeneous phantom with RW3 material arranged according to Table 2 are irradiated for 100 MU with a dose rate of 400 MU/min. Second, an inhomogeneous female Rando phantom

(Alderson Research Laboratories Inc. Stanford. CT, USA) are irradiated in the abdomen area of the size 10×10 cm<sup>2</sup> for 242 MU with a dose rate of 400 MU/min, and the gantry angle was set at 0 degrees. Replanning was shown in Figure 4(a) and the setup of the RANDO phantom as shown in Figure 4(b).

For IMRT, the phantom is irradiated following a real cancer case, but the gantry angle is normalized to zero degrees and the patient is transformed into a homogeneous phantom with a thickness of 10 cm. All phantoms are scanned on a CT simulator and the calculated dose distribution are exported in DICOM format. The EPID and the actual dose distribution images were set to a dimension of 384×512.

$$Profile_{GRID} = Pixel\ size_{EPID} \times \frac{SAD}{SDD} \quad (3)$$

$$Normalization\ Profile_{inline} = S_{x, \frac{512}{2}} \times \frac{100}{\max\left(S_{x, \frac{512}{2}}\right)} \quad (4)$$

$$Nomalization\ Profile_{crossline} = S_{\frac{384}{2}, y} \times \frac{100}{\max\left(S_{\frac{384}{2}, y}\right)} \quad (5)$$

Since the position of the EPID detector is 50 cm below the isocenter plane (see Figure 1), the EPID images were magnified from its their original size. Therefore, the grid of the EPID images must be scaled back to its original size using Equation 3. The pixel value of the EPID images is not comparable to the dose value of the dose distribution images. Therefore, for profile analysis purposes, both images need to be normalized using Equation 4 and Equation 5. Each EPID profile was analyzed using Full Width Half Maximum (FWHM). Furthermore, the discrepancy between the EPID and TPS profiles was calculated based on the percentage of deviations shown in Equation 6.

$$Percentage\ of\ deviation = \frac{Standard\ deviation}{Reference\ value} \times 100 \quad (6)$$

## Results

### Conversion of cine EPID pixel value to dose by AI model

The model is obtained after carrying out the training process, the data that has been separated for testing is reused for validation using the gamma index 3%/3mm, and the testing data is converted from pixel to dose using the model and compared to the TPS dose distribution image. Figure 5 shows that the average gamma index is 45.17%, with the highest value only reaching 92.40% ±28.14%.

Figure 6 tries to group the distribution of the gamma index results, there were 10 groups based on the percentage range of accuracy. It shows us from 381 images that were tested, there were 45 images above 90% or 11.8% of the total cases tested, while the largest group is the accuracy between 20-30%. It reaches 125 cases or 32.8% of the total cases tested. These results indicate that the model is successful in providing direct conversion of pixels in EPID cine images to doses. These results are new proposals and cannot be compared with other studies.

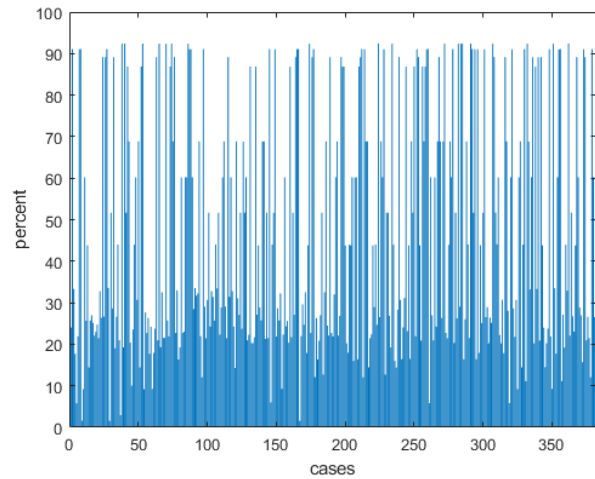


Figure 5. Gamma index 3%/3mm for 381 different cases

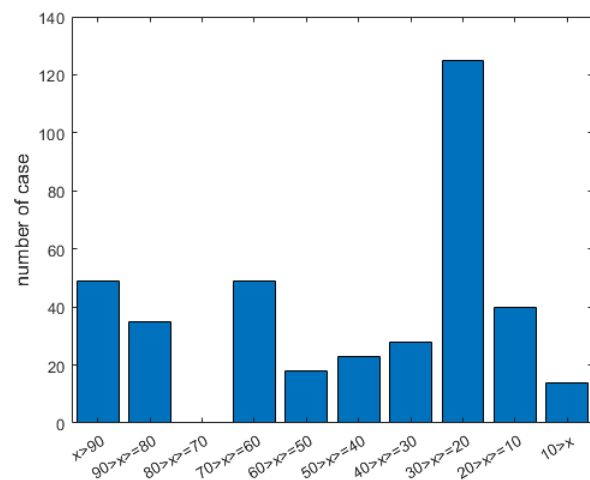


Figure 6. Gamma passing rate group

### The characteristics of Cine EPID Images

Based on Figure 7(a), the correlation between the number of cine EPID images (y-axis) vs. dose rate (MU/min) (x-axis) is negative linear, with the equation being  $y = -0.066x + 45.000$ ; it means the number of images decreases as the dose rate increases. Because the data taken is only 4 points, the dose rate pattern still looks quite linear, but it is still necessary to anticipate a model that fails to convert the pixel value into a dose because decreasing the number of images at a high dose rate will reduce the pixel value that is read after equation 2 is completed.

Furthermore, Figure 7(b) shows that the correlation between the number of cine EPID images versus MU tends to be linear. The equation  $y = 0.177x + 0.036$  indicates that the number of images increases as the MU increases. At a 400 MU/min dose rate, we found that EPID images increased every 5 MU. However, there were anomalies with no increases at MU 20, 60, 110, 145, 155, 195, and 240 that must be anticipated to reduce the possibility of the model failing to convert.

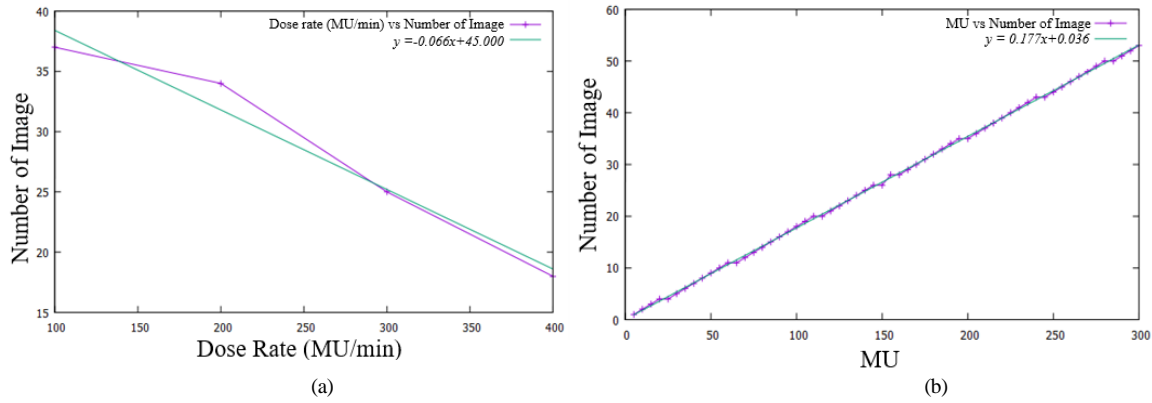


Figure 7. Relation between number of Cine EPID images vs (a) dose rate (MU/min) and (b) MU

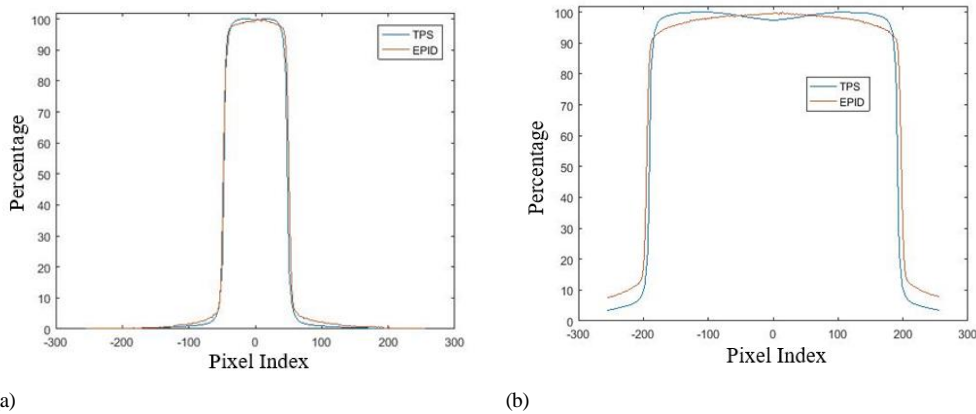


Figure 8. Crossline profile of the homogenous phantom between TPS vs EPID (a) 5×5 cm<sup>2</sup> (b) 20×20 cm<sup>2</sup>

Figure 8 is an example of an inline profile (pixel index versus percentage at the central axis in inline direction) of EPID versus TPS in a homogeneous phantom. Figure 8(a) shows that the EPID image profile displays significant similarities in the field size of 5×5 cm<sup>2</sup>. On the other hand, as illustrated in Figure 8(b), the EPID image does not show similarities to the TPS image in a field greater than 5×5 cm<sup>2</sup>, especially in the umbra section (below 20%) and the horn shape.

Figure 9 shows that the EPID image cannot read a large field such as a 20×20 cm<sup>2</sup> because of the EPID detector's limited size. The inability of the detector to read the entire area of such a size will indicate the failure to construct dosimetry based on EPID images.

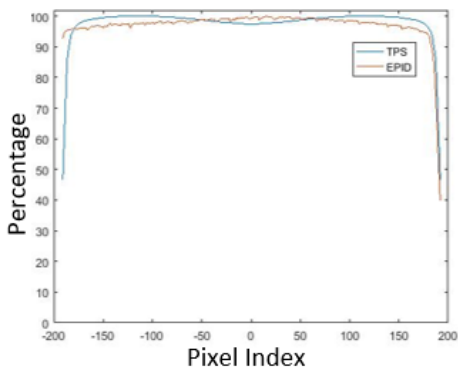


Figure 9. Inline profile on homogenous phantom with field size 20×20 cm<sup>2</sup>

Tables 4 and 5 shows the comparison between EPID and TPS images at the isocenter in the RANDO phantom with conformal radiotherapy technique and homogeneous phantom with IMRT technique. Both tables show inline and crossline profiles from EPID are similar to TPS. In the RANDO phantom, FWHM measurements on the inline and crossline profile showed a difference of ± 1.367% and ± 1.580%, respectively. Similar in the IMRT technique, the inline and crossline profiles show different differences just ± 0.794% and ± 1.925%, respectively.

Table 4. Comparison between EPID and TPS images at the isocenter in the RANDO female phantom

Parameter	FWHM (mm)	
	Inline	Crossline
TPS	100.493	100.370
EPID	102.435	102.613
Percentage deviation (%)	±1.367	±1.580

Table 5. Comparison between EPID and TPS image at the isocenter in the homogeneous phantom with the IMRT technique

Parameter	FWHM (mm)	
	Inline	Crossline
TPS	103.390	113.982
EPID	104.552	117.085
Percentage deviation (%)	±0.794	±1.925

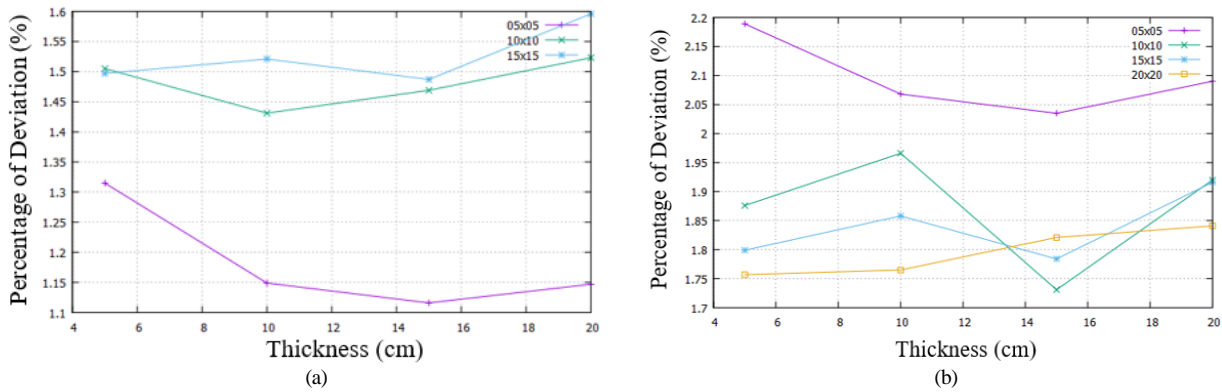


Figure 10. Percentage of deviation between VS Thickness of homogeneous phantom (a) inline profile; (b) crossline profile

Figure 10 shows the comparison between thickness and percentage of deviation from FWHM in inline and crossline profiles, color line indicates the field size variation. Figure 10 shows there is no dominant pattern found in terms of increasing thickness and field size of homogeneous phantom versus discrepancies in FWHM measurement. This indicates that the field size of the EPID and TPS images are similar. Furthermore, Figure 11(a) compares the inline profile of EPID and TPS of the female RANDO phantom with the conformal radiotherapy technique, it is demonstrating that the profile does not fit both the umbra region and horn region. It also has a large ripple resulting from the material responses in the detector and the backscattering of the attenuator. Figure 11(b) shows the inline profile between EPID and TPS in the homogeneous phantom with the IMRT technique. In this case, the profile of EPID and TPS is a much better match than on RANDO phantoms as well as in the umbra section.

### Discussion

Based on this study, the AI model has been successfully implemented and great opportunity to be used as a technique for converting pixel values in EPID images into doses directly but needs improvement before being used in daily measurements. Due to limited computational resources, the model has only been run on 15 epochs.

The current model used is possible to be improved, starting with adding dropouts, number of layers and epochs, or making variations in loss function techniques. The loss function is a function that helps AI to determine whether the weighted value is appropriate or not. Mean squared error is one of the most frequently used to measure the similarity of two images. In the future, it is possible to use the gamma index as a loss function, but large computational resources are required to do it.

Besides improving the model, adding data sets can improve the accuracy and reduce over fitting of the conversion of EPID pixel values into doses. Furthermore, image processing to in the preprocessing section also can be employed before the data is trained. It is intended that the data learned by AI is does not

contain noise which often causes AI to fail to learn data patterns correctly.

Besides CNN, numerous AI models have possibility to facilitate conversion from pixel value to dose, such as U-Net, this model has been used as a correction technique for EPID dose distribution in the umbra (dose to dose correction not conversion) (21,24). Another example model is a generative adversarial network (GAN), this model has a good result of image-to-image translation cases (22). Basically, every model used to improve image quality could be used to conversion because it utilizes image regression techniques, it regresses between the value of the source data to the target data. Due to the complexity of cine EPID images, finding the most appropriate AI model will be a challenge for researchers in radiotherapy.

Focus on the relationship between the number of cine EPID images to MU, Figure 7(b) shows that the response of cine mode is approximately related to the loss of 1 frame per irradiation. The response comes up to a linear dependence with increasing MU, but random anomalies in several MU's occurred, namely at 20, 60, 110, 145, 155, 195, and 240. Referring to Equation 2, the loss of 1 frame will greatly affect the result of the sum of the pixel values of the entire cine EPID image. because of that, inconsistency of frame loss will cause the AI model to misinterpret pixel values to dose.

Furthermore, Figure 8 shows the EPID images do not match TPS in the umbra region and horn shape in a homogeneous phantom with a conformal radiotherapy technique. The horn shape first appears at a field 5x5 cm<sup>2</sup> and arises dependent on increasing field size. This is similar to the study by Peca et al, their which converts pixel values to doses with an empirical equation involving tissue maximum ratio (TMR) values and adds corrections to the horn and umbra sections (11). On the other hand, Figure 11(a) shows that in the inhomogeneous phantom at field 10x10 cm<sup>2</sup>, the horn in the TPS image does not exist.

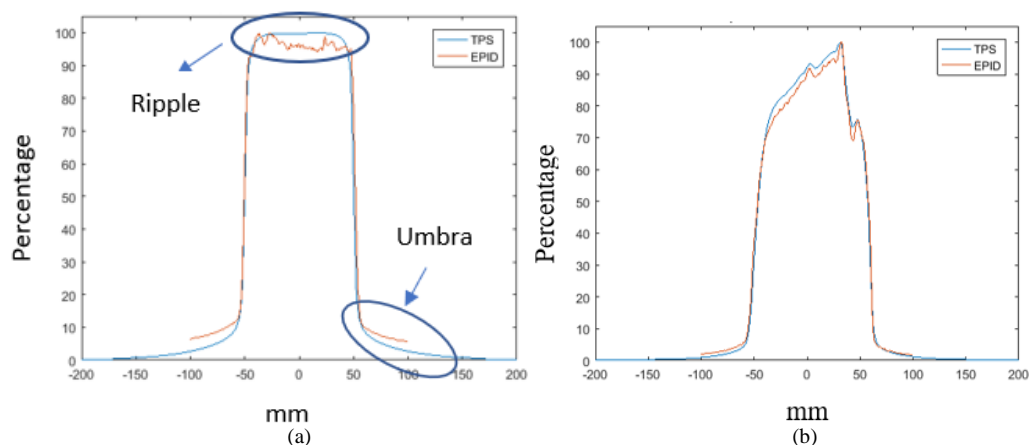


Figure 11. Inline profile between EPID vs TPS: (a) Rando female phantom (b) IMRT technique

This proves that adding horn correction for all cases will decrease accuracy when the actual dose profile has no horn. Moreover, in Figure 11(b), the beams profile of the IMRT technique for homogeneous phantom has better matches than other techniques. It is caused by the images taken using IMRT have having no horn forms in their profiles. The results also show that horn correction for dosimetry based on EPID image in the IMRT technique is not required.

Figure 9 shows that making dosimetry based on EPID images must pay attention to the size of the detector, based on our calculations, the maximum limit of a-Si 1000 EPID placed at SDD 150 cm and the organ target at SAD 100 cm can only capture a maximum field size of  $10 \times 13.33 \text{ cm}^2$  (25), beyond that, there will be truncated parts such as umbra, penumbra, etc. Increasing the SDD position is not recommended as it will increase the backscattering of the attenuator and material within the detector itself (1).

Tables 4,5 and Figure 10 confirms the results of McCurdi's research which states that there is no problem with the field size of the EPID image against the reference. the percentage of discrepancy at FWHM measurement also shows under 2.2% between EPID vs TPS profile. In addition, the differences in the results of FWHM measurements on the inline and crossline profiles indicate that the detector's resolution has a big impact on the image. EPID A-Si 1000 has a different resolution in the  $x$  and  $y$  direction, as explained in Table 1. Therefore, using a detector with a different resolution is not recommended to build dosimetry because of the difficulty of correcting the EPID images. This also clarifies previous research that proved EPID A-Si 1200 provides more accurate measurements than EPID A-Si 1000; one of the reasons is the detector has an equal resolution in inline and crossline profiles (26).

Moreover, every beam profile in EPID images has a ripple that occurs due to backscattering between the detector material, the attenuator, and the detector's response. It is also a consequence by of the pixel sensitivity variation and off-axis dose-response of an EPID. This effect has been described by Greer et al.

(27). In previous research by Ding et al., a correction was added with flood field and dark field images (28).

## Conclusion

The study shows that the AI model has been successfully implemented to convert the pixel value of EPID images to dose. The comparison between the dose calculated by AI model and TPS reached  $92.40\% \pm 28.14\%$ . gamma passing rates at 3% / 3mm, so it needs further study to improve the result. Moreover, the inconsistency of increasing the number of cine EPID images with increasing MU and dose rate needs to be resolved in order to avoid conversion errors by the AI model. Ripple correction (artifact) that occurs in the EPID image due to backscattering also needs to be added to the preprocessing, so that the model only learns the actual pixel value pattern. In the end, considering that the horn and umbra appear in conformal radiotherapy but not in IMRT, the AI model must be built based on the irradiation technique, different irradiation techniques must be retrained on the model.

## Acknowledgment

This study was supported by the Universitas Indonesia PUTI research Grant with contract number NKB-1665/UN2.RST/HKP.05/00/2020.

## References

1. Tan YI. 2D transit dosimetry using electronic portal imaging device [Thesis]. University of Glasgow; 2016.
2. Van Elmpt W, McDermott L, Nijsten S, Wendling M, Lambin P, Mijnheer B. A literature review of electronic portal imaging for radiotherapy dosimetry. *Radiotherapy and Oncology*. 2008;88(3):289–309.
3. Yip S, Rottmann J, Berbeco R. The impact of cine EPID image acquisition frame rate on markerless soft-tissue tracking. *Medical Physics*. 2014;41(6):061702.
4. Mans A, Wendling M, McDermott LN, Sonke JJ, Tielenburg R, Vijlbrief R, et al. Catching errors with in vivo EPID dosimetry. *Medical Physics*. 2010;37(6):2638–44.

5. Tan YI, Metwaly M, Glegg M, Baggarley SP, Elliott A. A dual two dimensional electronic portal imaging device transit dosimetry model based on an empirical quadratic formalism. *British Journal of Radiology*. 2015;88(1051):20140645.
6. Peca S, Brown DW. Two-dimensional in vivo dose verification using portal imaging and correlation ratios. *Journal of Applied Clinical Medical Physics*. 2014;15(4):117–28.
7. Wendling M, McDermott LN, Mans A, Sonke JJ, van Herk M, Mijnheer BJ. A simple backprojection algorithm for 3D in vivo EPID dosimetry of IMRT treatments. *Medical Physics*. 2009;36(7):3310–21.
8. Wendling M, Louwe RJW, McDermott LN, Sonke JJ, van Herk M, Mijnheer BJ. Accurate two-dimensional IMRT verification using a back-projection EPID dosimetry method. *Medical Physics*. 2006;33(2):259–73.
9. Wendling M, McDermott LN, Mans A, Olaciregui-ruiiz Í, Pecharromán-gallego R, Sonke J, et al. In aqua vivo EPID dosimetry In aqua vivo EPID dosimetry. 2012;367.
10. Piermattei A, Fidanzio A, Stimato G, Azario L, Grimaldi L, D'Onofrio G, et al. In vivo dosimetry by an aSi-based EPID. *Medical Physics*. 2006;33(11):4414–22.
11. Peca S, Brown DW, Smith WL. A Simple Method for 2-D In Vivo Dosimetry by Portal Imaging. *Technology in Cancer Research and Treatment*. 2017;16(6):944–55.
12. Winkler P, Hefner A, Georg D. Dose-response characteristics of an amorphous silicon EPID. *Medical Physics*. 2005;32(10):3095–105.
13. Mccurdy BMCC. Dosimetry in radiotherapy using a-Si EPIDs: Systems, methods, and applications focusing on 3D patient dose estimation. *Journal of Physics: Conference Series*. 2013;444(1).
14. Bridge P, Bridge R. Artificial Intelligence in Radiotherapy: A Philosophical Perspective. *Journal of Medical Imaging and Radiation Sciences*. 2019;50(4):S27–31.
15. Thompson RF, Valdes G, Fuller CD, Carpenter CM, Morin O, Aneja S, et al. Artificial intelligence in radiation oncology: A specialty-wide disruptive transformation? *Radiotherapy and Oncology*. 2018;129(3):421–6.
16. Poortmans PMP, Takanen S, Nader G, Meattini I. Winter is over : The use of Arti fi cial Intelligence to individualise radiation therapy for breast cancer \*. *The Breast*. 2020;49:194–200.
17. Jarrett D, Stride E, Vallis K, Gooding MJ. Applications and limitations of machine learning in radiation oncology. *British Journal of Radiology*. 2019;92(1100):1–12.
18. Kalet AM, Luk SMH, Phillips MH. Radiation Therapy Quality Assurance Tasks and Tools: The Many Roles of Machine Learning. *Medical Physics*. 2020;47(5):e168–77.
19. Luo Y, Chen S, Valdes G. Machine learning for radiation outcome modeling and prediction. *Medical Physics*. 2020;47(5):e178–84.
20. Sadeghnejad Barkousaraie A, Ogunmolu O, Jiang S, Nguyen D. A fast deep learning approach for beam orientation optimization for prostate cancer treated with intensity-modulated radiation therapy. *Medical Physics*. 2020;47(3):880–97.
21. Ronneberger O, Fischer P, Brox T. U-Net: Convolutional Networks for Biomedical Image Segmentation. 2015;1–8.
22. Armanious K, Jiang C, Abdulatif S, Küstner T, Gatidis S, Yang B. Unsupervised medical image translation using Cycle-MeDGAN. *European Signal Processing Conference*. 2019;2019;1-5.
23. Liu Z, Yan WQ, Yang ML. Image denoising based on a CNN model. In: *Proceedings - 2018 4th International Conference on Control, Automation and Robotics, ICCAR 2018*. 2018.
24. Olaciregui-Ruiz I, Torres-Xirau I, Teuwen J, van der Heide UA, Mans A. A Deep Learning-based correction to EPID dosimetry for attenuation and scatter in the Unity MR-Linac system. *Physica Medica*. 2020;71:124–31.
25. Podgorsak EB. *Radiation Oncology Physics: A Handbook for Teachers and Students*. Vienna; 2005.
26. Mhatre V, Pilakkal S, Chadha P, Talpatra K. Dosimetric Comparison of a-Si 1200 and a-Si 1000 Electronic Portal Imager for Intensity Modulated Radiation Therapy ( IMRT ). *Journal of Nuclear Medicine & Radiation Therapy*. 2018;9(1):1–6.
27. Greer PB. Correction of pixel sensitivity variation and off-axis response for amorphous silicon EPID dosimetry Correction of pixel sensitivity variation and off-axis response for amorphous silicon EPID dosimetry. 2014;3558(2005).
28. Ding A, Xing L, Han B. Development of an accurate EPID-based output measurement and dosimetric verification tool for electron beam therapy. *Medical Physics*. 2015;42(7):4190–8.